Negative Poisson's ratio and semisoft elasticity of smectic-*C* liquid-crystal elastomers

A. W. Brown and J. M. Adams
SEPnet and the Department of Physics, Faculty of Engineering and Physical Sciences, University of Surrey, Guildford GU2 7XH, United Kingdom

(Received 27 July 2011; revised manuscript received 9 December 2011; published 13 January 2012)

Models of smectic-*C* liquid-crystal elastomers predict that they can display soft elasticity, in which the shape of the elastomer changes at no energy cost. The amplitude of the soft mode and the accompanying shears are dependent on the orientation of the layer normal and the director with respect to the stretch axis. We demonstrate that in some geometries the director is forced to rotate perpendicular to the stretch axis, causing lateral expansion of the sample—a negative Poisson's ratio. Current models do not include the effect of imperfections that must be present in the physical sample. We investigate the effect of a simple model of these imperfections on the soft modes in monodomain smectic-*C* elastomers in a variety of geometries. When stretching parallel to the layer normal (with imposed *strain*) the elastomer has a negative stiffness once the director starts to rotate. We show that this is a result of the negative Poisson's ratio in this geometry through a simple scalar model.

DOI: 10.1103/PhysRevE.85.011703 PACS number(s): 61.30.Vx, 83.80.Va, 46.32.+x, 62.20.dj

I. INTRODUCTION

Liquid-crystal elastomers (LCEs) are soft solids composed of flexible polymers, with attached liquid-crystalline mesogens, crosslinked into a network [1]. A variety of liquid-crystalline phases of LCEs have been synthesized, including the nematic and smectic phases. The nematic phase undergoes deformation at no energy cost, known as soft elasticity [2] in both monodomain samples stretched perpendicular to the director [3] and in some types of polydomain samples [4–6]. Soft elasticity in nematic elastomers requires several sympathetic shears to develop during the deformation as the director rotates. The deformation of the sample must also obey the boundary conditions imposed by the clamps. Thus, the sample forms a striped microstructure on the micrometer length scale consisting of domains in which the director rotates in opposite directions in adjacent domains [7]. Without this microstructure soft deformations would not be possible. In nematics this microstructure has been observed in some detail experimentally [8], and its mathematical properties described [9]. Theoretically an ideal nematic LCE should be perfectly soft; however, in practice a small force must be applied to deform the LCE. This semisoft behavior is due to various imperfections in the elastomer and can be incorporated into theoretical models by the addition of a semisoft energy term that penalizes rotation of the director with respect to the rubber matrix [10].

Smectic LCEs have been fabricated in both the smectic-*A* (Sm-*A*) and smectic-*C* (Sm-*C*) phases, and with both main chain [11] and side chain [12] architectures. The mechanical behavior of the side chain systems can be modeled by adding in the embedded smectic layers to the nematic elasticity free energy [13,14]. Sm-*A* elastomers with a high degree of smectic order exhibit a sharp change in their elastic deformation when deformed parallel to the layer normal. They are extremely anisotropic materials, with a Young's modulus a factor of 100 times larger parallel to the layer normal compared with perpendicular directions [12,15,16]. However, the response of smectic elastomers depends on the chemistry, the crosslinking procedure, and domain sizes in the sample [17]. Theoretical models of the Sm-*A* phase have been successful in modeling the mechanical behavior of side chain systems. In contrast to the nematic phase the Sm-*A* phase does not show any soft elastic behavior because the director is locked parallel to the layer normal. The elastic behavior of Sm-*C* elastomers is predicted to be more complex. The director is free to rotate on a cone around the layer normal, with fixed tilt angle as shown Fig. 1(a). As a consequence it is predicted to have a soft elastic mode just as in nematic elastomers [18,19]. A more complicated combination of shears is required in Sm-*C* soft modes. As a result of the compatibility requirements between these deformations a far more restricted set of tensile geometries are predicted to deform softly with clamped boundary conditions [20].

To test these theoretical results experimentally, a monodomain must be produced which requires alignment of both the layer normal and the director. Using a two-stage crosslinking method, the director field can be uniformly aligned [21]. However, the layer normals are tilted at a fixed angle on a cone around the director. We will refer to this as a *pseudo-monodomain* [see Fig. 1(b)] [22] in order to distinguish it from a monodomain, which has both the layer normal and the director uniformly aligned, and a polydomain, which has random director and layer normal alignment. The layer normals in the pseudo-monodomain can be aligned by a second uniaxial deformation perpendicular to one of the layer normals [23], or alternatively by a shear deformation perpendicular to the director [24]. To our knowledge no mechanical experiments on monodomain Sm-*C* elastomers have been reported, perhaps because of the difficulty in aligning these samples. However, the spontaneous deformations associated with changing the phase of the elastomer from Sm-*A* to Sm-*C* have been observed [25]. Many more experiments have been carried out on the more accessible polydomain system [11,26]. Unfortunately, as with many polydomain systems, this is more difficult to model theoretically. However, these experiments on the main chain Sm-*C* pseudo-monodomain show that when stretching the sample perpendicular to the director, the layer normals rotate toward the extensional axis. If the smectic layers behaved as embedded planes (a key assumption in the model of side chain smectic LCEs), then they would rotate away from

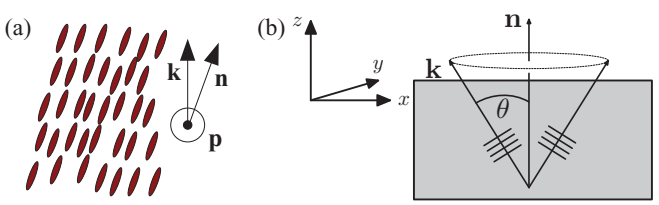

FIG. 1. (Color online) (a) The layer normal **k** and director **n** in the Sm-C phase, and the transverse dipole orientation **p** in the Sm-C^* phase (polymer chains not shown). (b) The director and layer normals in a pseudo-monodomain.

the extensional axis. This behavior is thought to arise because of the unfolding of hairpins in the main chain system [27].

The director reorientation in soft modes may be particularly important for the electromechanical properties of chiral Sm-C^* phase elastomers [28]. In these systems the mesogenic units have a permanent transverse dipole, which on average is oriented perpendicular to both the director and the layer normal $\mathbf{p} = \mathbf{n} \times \mathbf{k}$ as shown in Fig. 1(a). The coupling between the macroscopic mechanical deformations and the microscopic orientation of these dipoles results in their piezoelectric properties. These materials show both the direct piezoelectric effect in pseudo-monodomains [29], as well as the inverse piezoelectric effect [30]. Spontaneous polarization of pseudo-monodomains has also been reported [22].

Under a tensile load materials with a negative Poisson's ratio produce a transverse expansion. This property is useful in gasket applications and has been produced in cellular materials with a reentrant structure [31]. There is interest in negative stiffness materials for applications such as stiffening composites [32] and creating metamaterials having a negative refractive index to sound waves [33]. Both negative Poisson's ratio and negative stiffness are predicted in Sm-C elastomers by the model described here.

This paper is organized as follows. We will describe the model of Sm-C elastomers that will be used in Sec. II, and show that the soft modes in this model have negative incremental Poisson's ratio in some geometries. In Sec. III we will illustrate the effect of the semisoft elastic term in four different geometries. We will then summarize the effect of this term and discuss the model predictions in relation to the mechanical experiments in polydomains in Sec. IV.

II. MODEL FREE ENERGY

The model of a Sm-C elastomer that will be used here is described in Refs. [34,35]. The free energy has contributions from the nematic elasticity $F_{\rm nem}$, smectic layer spacing $F_{\rm sm}$, and the energy penalty for changing the tilt of the director with respect to the layer normal $F_{\rm tilt}$. The nematic elasticity is given by

$$F_{\rm nem} = \tfrac{1}{2}\mu {\rm Tr}\left[\underline{\underline{\lambda}} \cdot \underline{\underline{\ell}}_0 \cdot \underline{\underline{\lambda}}^T \cdot \underline{\underline{\ell}}^{-1}\right], \tag{1}$$

where μ is the rubber shear modulus, and $\underline{\underline{\lambda}}$ is the deformation gradient. The step length tensor before the deformation has been applied is $\underline{\underline{\ell}}_0 = \underline{\underline{\delta}} + (r-1)\mathbf{n}_0\mathbf{n}_0$, with $\mathbf{n}_0$ the initial director, $\underline{\underline{\delta}}$ the unit tensor, and r the polymer anisotropy. The current step length tensor is denoted by $\underline{\underline{\ell}}$, and its inverse by $\underline{\underline{\ell}}^{-1} = \underline{\underline{\delta}} + (1/r - 1)\mathbf{nn}$, with **n** the final director. In principle a Sm-C elastomer should have a biaxial shape tensor for the polymer backbone because its shape may be affected by both the director alignment and the layer normal direction. As a first approximation we will treat it as uniaxial here, depending only on the director orientation **n**. Biaxial soft modes in Sm-A elastomers [18] and the effect of biaxiality in Sm-C soft modes [28] are considered elsewhere. We will also assume that the nematic and smectic order parameters remain fixed throughout the deformation.

It is assumed that the smectic layers are embedded in the rubber matrix, so that the corresponding layer normals **k** will deform like embedded planes:

$$\mathbf{k} = \frac{\underline{\underline{\lambda}}^{-T} \cdot \mathbf{k}_0}{|\underline{\underline{\lambda}}^{-T} \cdot \mathbf{k}_0|}, \tag{2}$$

where $\mathbf{k}_0$ is the initial layer normal. The layer spacing is penalized by the smectic liquid-crystal modulus B:

$$F_{\rm sm} = \tfrac{1}{2}B\left(\frac{d}{d_0} - \frac{\cos\theta}{\cos\theta_0}\right)^2, \tag{3}$$

where d is the final layer spacing, d_0 is the initial layer spacing, and $d/d_0 = 1/|\underline{\underline{\lambda}}^{-T} \cdot \mathbf{k}_0|$. $F_{\rm sm}$ describes the free energy penalty for deviations of the layer spacing away from that required to accommodate the smectic mesogens. For tilted smectic mesogens, the required layer spacing is $\cos\theta/\cos\theta_0$, where the tilt angle with respect to the layer normal is θ_0 in the initial state and θ in the current state. The free energy term that penalizes the deviation of the director from a tilt angle θ_0 is

$$F_{\rm tilt} = \tfrac{1}{2}a_t[\cos^2\theta_0 - (\mathbf{n}\cdot\mathbf{k})^2]^2, \tag{4}$$

where a_t is the tilt modulus and $\mathbf{n}\cdot\mathbf{k} = \cos\theta$.

It will be assumed here that the bulk modulus of the rubber is much larger than the shear, tilt, and smectic moduli, so that the deformation gradient obeys $\det[\underline{\underline{\lambda}}] = 1$; hence it conserves volume. Typically the smectic layer modulus is very large compared to the rubber shear modulus, i.e., $B \gg \mu$ (at least in smectic elastomers of a similar type to that of Nishikawa *et al.* [15]), so that the layer spacing remains almost fixed. The tilt modulus is also large compared to the shear modulus $a_t \gg \mu$, so that the tilt angle remains close to θ_0 [36].

A. Soft elasticity

The free energy outlined above permits the subset of the nematic soft modes that maintain the layer spacing. There is only one soft mode that satisfies this (up to a global rotation), and it corresponds to a rotation of the director about the layer normal [18,19]. We summarize some of the properties of this soft mode here, as they are crucial in understanding the semisoft response of the elastomer.

We assume that the layer normal points along the **z** direction, and the director is tilted into the **y** direction; i.e., $\mathbf{k}_0 = \mathbf{z}$ and $\mathbf{n}_0 = \mathbf{z}\cos\theta_0 + \mathbf{y}\sin\theta_0$ in the starting state. The soft modes can be parameterized by the angle ϕ which gives the rotation of the director $\mathbf{n}_0$ around the layer normal toward

the **x** direction. The deformation matrix is given by [18]

$$\begin{pmatrix} \frac{1}{a(\phi)} & (1-\frac{\rho}{r})\frac{\sin 2\phi}{2a(\phi)} & \frac{(r-1)\sin 2\theta_0}{2\rho}\left[\sin\phi - \left(1-\frac{\rho}{r}\right)\frac{\sin 2\phi}{2a(\phi)}\right] \\ 0 & a(\phi) & \frac{(r-1)}{2\rho}\sin 2\theta_0[-a(\phi)+\cos\phi] \\ 0 & 0 & 1 \end{pmatrix}, \tag{5}$$

where

$$\rho = \sin^2\theta_0 + r\cos^2\theta_0, \tag{6}$$

$$a(\phi) = \sqrt{\cos^2\phi + \frac{\rho}{r}\sin^2\phi}. \tag{7}$$

The deformation components as a function of rotation angle are illustrated in Fig. 2. The soft mode representation shown in Fig. 2(c) uses the undeformed Sm-*C* phase as the reference state. The high temperature isotropic phase is the most natural reference state for the nematic elastomer free energy [37]. This alternative reference state can also be used to provide a mathematically simpler free energy to analyze for the Sm-*C* elastomer phase [20].

The soft mode in Eq. (5), denoted by $\underline{\lambda}_{\text{soft}}$, can be transformed to different starting configurations of the director and layer normal by a set of rotation matrices. This is described in Appendix A for the case of stretching parallel to the layer normal in the $\mathbf{k}_0 = \mathbf{x}$ direction, when $\mathbf{n}_0 = \cos\theta_0\mathbf{x} + \sin\theta_0\mathbf{y}$. Although the result is analytic, the algebra is not instructive and is not presented here. The components of the deformation matrix for this geometry are illustrated in Fig. 3. The λ_{zz} component increases with imposed λ_{xx}; i.e., the sample expands

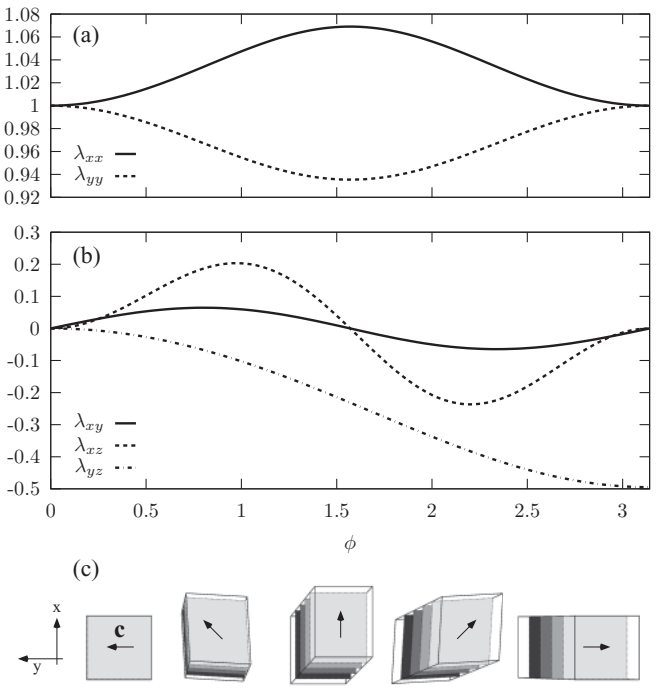

FIG. 2. For the parameter values $r = 2$ and $\theta_0 = 0.5$ radians, (a) shows the diagonal components of the deformation matrix, (b) shows the shear components, and (c) shows an illustration of the deformations on the LCE, together with the component of the director perpendicular to the layer normal, **c**.

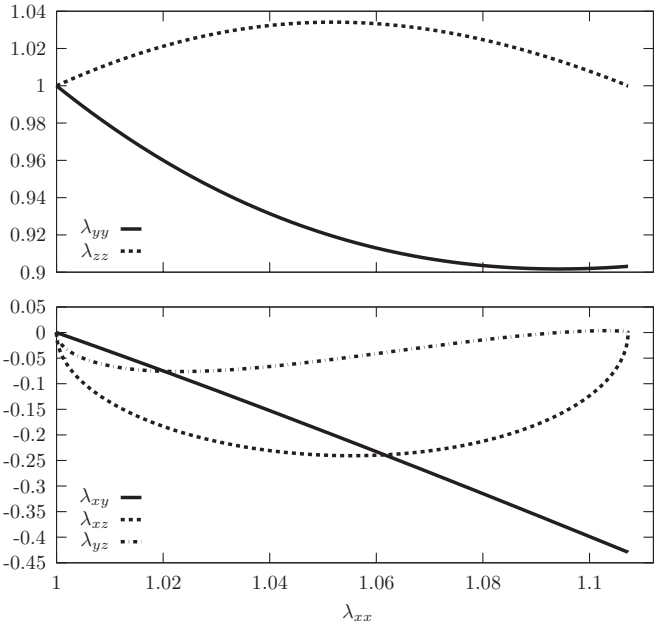

FIG. 3. The components of the upper triangular deformation matrix for the Sm-*C* soft mode stretching parallel to the layer normal, with $r = 2$ and $\theta_0 = 0.5$ radians. Initially $\mathbf{k}_0 = \mathbf{x}$ and $\mathbf{n}_0 = \cos\theta_0\mathbf{x} + \sin\theta_0\mathbf{y}$.

in the direction perpendicular to the imposed elongation. This is because the constraint requiring a fixed angle between the layer normal and director results in the director rotating in the z direction. The sample then expands to accommodate the anisotropic chain shape, as shown in Fig. 4. This illustrates an unusual property of some Sm-*C* soft modes: their *negative* Poisson's ratio. To our knowledge this mechanism for negative Poisson's ratio has not been reported before. Alternative mechanisms of producing auxetic behavior based on modifying the attachment of mesogens to the polymer backbone in smectic LCEs have been proposed and investigated experimentally [38,39]. The microstructure formed by LCEs during deformation may prevent the observation of negative Poisson's ratio for some deformations. This is discussed further in Sec. IV.

For isotropic materials, the Poisson's ratio must be in the range $-1 < \nu < 0.5$. LCEs are anisotropic materials and so have Poisson's ratios outside this range. As the materials considered here are volume conserving, the Poisson's ratio in the y direction is $\nu_{yy} = 1 - \nu_{zz}$. When stretching parallel to the layer normal, the Poisson's ratio for $\theta_0 > 0$ is given by

$$\nu_{zz} = -\left.\frac{d\lambda_{zz}}{d\lambda_{xx}}\right|_{\lambda_{xx}=1} = -\frac{1}{(r-1)\cos^2\theta_0}. \tag{8}$$

Substituting in typical values of $\theta_0 \sim 0.5$ radians and $r \sim 2$ for a side chain system produces $\nu \sim -1.3$. When compared with other auxetic materials [31] this is a more negative Poisson's ratio, corresponding to a larger rate of expansion (albeit in only one direction here). The extent of the soft mode in this

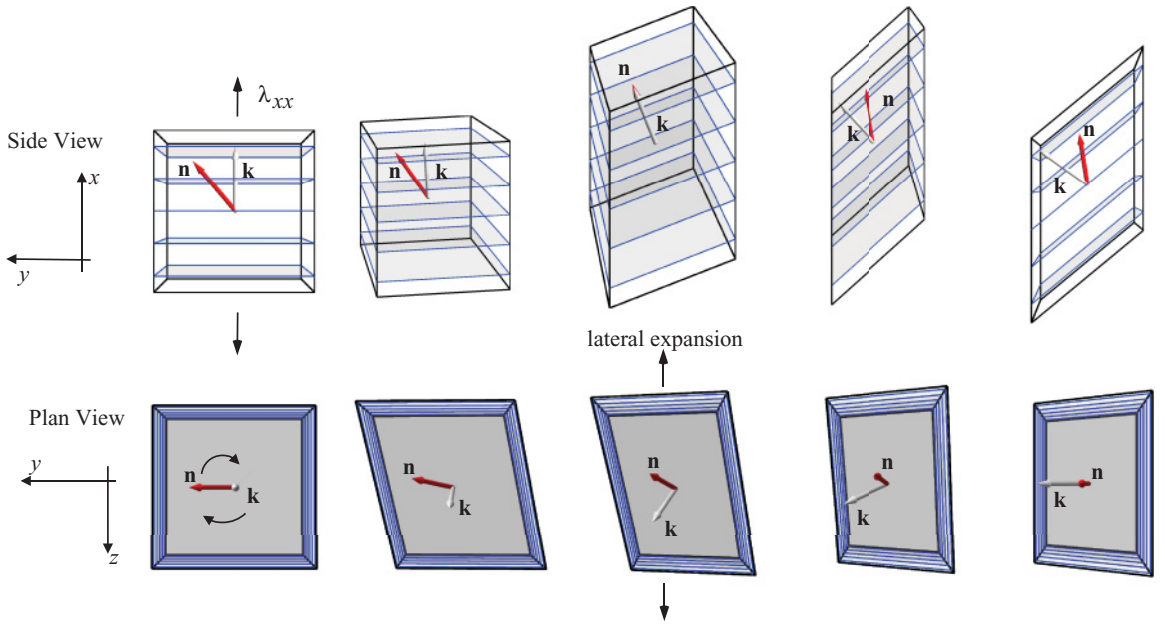

FIG. 4. (Color online) An illustration of the Sm-C elastomer deformation when stretching parallel to the layer normal. The director (red) moves out into the z direction perpendicular to the stretch axis, maintaining its tilt angle with respect to the layer normal (white) causing the elastomer to expand in the perpendicular direction.

geometry is

$$\lambda_{xx} = \sqrt{1 + \frac{(r-1)^2}{\rho^2} \sin^2 2\theta_0}\,. \tag{9}$$

To illustrate the expansion of the LCEs on elongation here, we will use the incremental Poisson's ratio (IPR) defined by

$$\nu_{zz} = -\frac{d\lambda_{zz}}{d\lambda_{xx}}, \tag{10}$$

where an elongation λ_{xx} is imposed and λ_{zz} is the transverse deformation.

B. Semisoft elasticity

Soft modes in ideal LCEs have zero energy cost, and so the sample requires no force to deform. In practice these materials have several sources of nonideal behavior, such as compositional fluctuations and crosslinking points that result in semisoft behavior. We will use the well known and general form (up to quadratic order) of semisoft elasticity in nematics [10]:

$$F_{ss} = \tfrac{1}{2}\alpha\mu \mathrm{Tr}\left[\underline{\underline{\lambda}} \cdot \left(\underline{\underline{\delta}} - \mathbf{n}_0\mathbf{n}_0^T\right) \cdot \underline{\underline{\lambda}}^T \cdot \mathbf{n}\mathbf{n}^T\right]. \tag{11}$$

Equation (11) is well founded in nematic LCEs and so serves as a starting point for smectic LCEs, where little is known about semisoft elastic terms. However, in Sm-C elastomers the semisoft term in the free energy could in principle involve any of the directions in the problem including the director and the layer normal. While a biaxial expression for the semisoft term could be developed we have used a uniaxial shape tensor $\underline{\underline{\ell}}$, so we will neglect these effects here for consistency.

Typical values of α are up to $\sim$0.1 in nematic LCEs, but they may be even larger in smectic LCEs [35]. We will look at the effect of varying α in Sm-C systems throughout this paper, which may change some other experimentally observable parameters, such as the ratio of shear moduli. A discussion of the effect of varying α in nematic LCEs can be found in [40].

The neo-Hookean elasticity formula

$$F_{ss} = \tfrac{1}{2}\alpha\mu \mathrm{Tr}[\underline{\underline{\lambda}} \cdot \underline{\underline{\lambda}}^{\mathrm{T}}] \tag{12}$$

term gives rise to the same qualitative behavior as Eq. (11). This expression is used as a regularizing perturbation for the numerical study of the ideally soft case [9]. A numerical study of the full semisoft free energy has also been carried out [41].

C. Numerical method

The free energy described in Eqs. (1), (3), (4), and (11) is subject to the nonlinear constraints that the director remains of unit length and that the layer normal deforms as an embedded plane Eq. (2). This constrained minimization can only be performed analytically in a few circumstances. Numerical minimization of this free energy using conventional methods often results in the location of only local minima. We have used a simulated annealing algorithm to minimize the total free energy, which finds the global free energy minimum more reliably. The constraint of the tilt angle of θ between the layer normal and the director can be encoded as

$$\mathbf{n} = \mathbf{c}\sin\theta + \mathbf{k}\cos\theta, \tag{13}$$

where the vector $\mathbf{c}$ is perpendicular to $\mathbf{k}$. A particular basis is required to express $\mathbf{c}$. It is convenient to use $\mathbf{c}_0$, the starting component of $\mathbf{n}_0$ perpendicular to $\mathbf{k}_0$, and $\mathbf{c}_0 \times \mathbf{k}_0$. The vector $\mathbf{c}$ can be expressed as

$$\mathbf{c} = \hat{\mathbf{a}}\cos\phi + \hat{\mathbf{b}}\sin\phi, \tag{14}$$

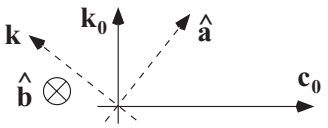

FIG. 5. An illustration of the vectors $\hat{\mathbf{a}}$ and $\hat{\mathbf{b}}$ used in the numerical calculations.

where $\hat{\mathbf{a}} \propto \mathbf{c}_0 - \mathbf{k}(\mathbf{c}_0 \cdot \mathbf{k})$ is a unit vector constructed from the component of $\mathbf{c}_0$ that is perpendicular to $\mathbf{k}$, and $\hat{\mathbf{b}}$ is perpendicular to both $\hat{\mathbf{a}}$ and $\mathbf{k}$ (Fig. 5); i.e., $\hat{\mathbf{b}} = \mathbf{k} \times \hat{\mathbf{a}}$. Hence in the initial configuration $\phi = 0$, and $\hat{\mathbf{a}} = \mathbf{c}_0$.

The simulated annealing algorithm then minimizes the free energy over ϕ,θ, and the required components of $\underline{\underline{\lambda}}$. The global minimum derived from this was then refined using a NAG sequential quadratic programming library routine. The imposed constraints are implemented using Lagrange multipliers. The results of this method are in good agreement with the results obtained from configurations that can be solved analytically.

III. ELONGATIONS OF Sm-*C* ELASTOMERS

We will consider four elongations to illustrate some of the behavior and to build up some intuition for semisoft Sm-*C* elastomers. The orientation of the layer normal and director in each case is shown in Fig. 6. The motivation for these different geometries is principally the experimental work on polydomain Sm-*C* elastomers [11] and the mathematical studies of the Sm-*C* free energy to find which soft deformations are permitted by the formation of compatible microstructures [20]. The elastic behavior of the polydomains is considerably more complicated. Understanding the elastic deformations of a semisoft monodomain is a useful step toward modeling the experimentally more accessible polydomain sample. We will ignore the effect of clamping at the boundaries, and

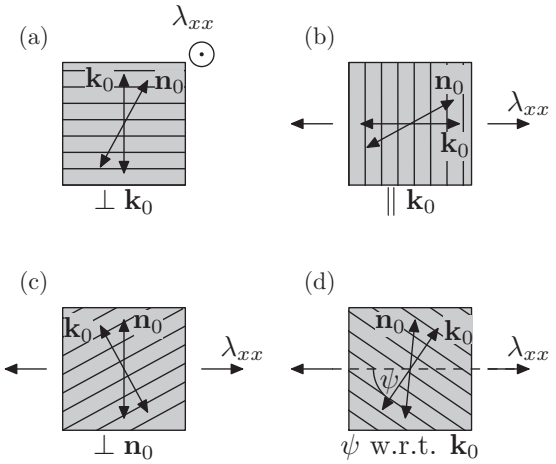

FIG. 6. The orientation of the director and layer normal for each of the elongations considered: (a) perpendicular to the layer normal (note that the director and layer normal are both perpendicular to the **x** direction initially), (b) parallel to the layer normal, (c) perpendicular to the director, and (d) at an angle ψ to the layer normal.

focus on the deformation of sheets of Sm-*C* elastomer whose mechanical properties will be dominated by the deformation of the material in the middle of the long sheet. We will consider elongations in the **x** direction, i.e., imposing the λ_{xx} component, together with the induced shear deformations. The appropriate deformation matrix is

$$\underline{\underline{\lambda}} = \begin{pmatrix} \lambda_{xx} & \lambda_{xy} & \lambda_{xz} \\ 0 & \lambda_{yy} & \lambda_{yz} \\ 0 & 0 & \lambda_{zz} \end{pmatrix}. \tag{15}$$

The yx and zx components are set to zero as they would be resisted by countertorques when applying a load in the **x** direction. The zy component can be set to zero by allowing suitable rotations about the **x** axis, along which the elastomer is stretched. In experiment, imposed stress ensembles are often used, which yield the same results when the stress-strain curve is monotonic. However, some of the stress-strain curves calculated here are nonmonotonic; hence there are several strain values for a single stress value. In this case there is a difference between the fixed stress and fixed strain ensembles, and for fixed stress a Maxwell construction must be used to determine the strain. This is described in [42] and briefly in Sec. IV.

The model has the parameters μ, a_t, B, r, and θ_0. Typically, $\theta_0 \sim 30^\circ$ [22], $B/\mu = b \sim 60$ in well ordered samples [12,15,17], $a_t/\mu = c \gtrsim 1$ and $\alpha \sim 0.1$ in smectics [35,36], and $r \sim 2$ in side chain liquid-crystalline polymers [1]. We will use these parameter values to illustrate the behavior of the model in what follows.

A. Elongation perpendicular to $\mathbf{n}_0$ and $\mathbf{k}_0$

First we consider an elongation deformation in the **x** direction, with the starting layer normal $\mathbf{k}_0 = \mathbf{z}$ and the starting director $\mathbf{n}_0 = \cos\theta_0 \mathbf{z} + \sin\theta_0 \mathbf{y}$, as illustrated in Fig. 6(a). In the absence of the semisoft term of Eq. (11) this deformation is as described in Sec. II A. The full free energy can be minimized numerically as explained in Sec. II C. The resulting stress-strain curve and the orientation of the director of this minimization are shown in Fig. 7 by the thick (green) lines. For the ideal Sm-*C* elastomer, this plateau ends at $\lambda_{xx} = \sqrt{\frac{r}{\rho}}$, as can be seen from the soft mode in Eq. (5). The plateau ends when the director has completed a rotation by $\pi/2$ around the layer normal. For nonzero values of α the onset of rotation of the layer normal is delayed, and it never finishes a full $\pi/2$ rotation. This is evident in the stress-strain curve, because the well defined stress plateau for $\alpha = 0$ becomes progressively less sharply defined. For $\alpha \sim 0.01$ there is a pronounced stress plateau, but for larger values of $\alpha \sim 0.1$ there is no plateau, merely a knee in the stress-strain curve. Figure 7 also shows the effect of reducing the tilt modulus c. The knee in the stress-strain curve becomes less pronounced, and the rubber hardens more slowly for larger values of λ_{xx}.

The retardation of the director rotation may be significant for piezoelectric response of these materials. There would be no piezoelectric response until the strain was above the threshold. The potential difference across the sample would be lower in semisoft samples because the alignment of the

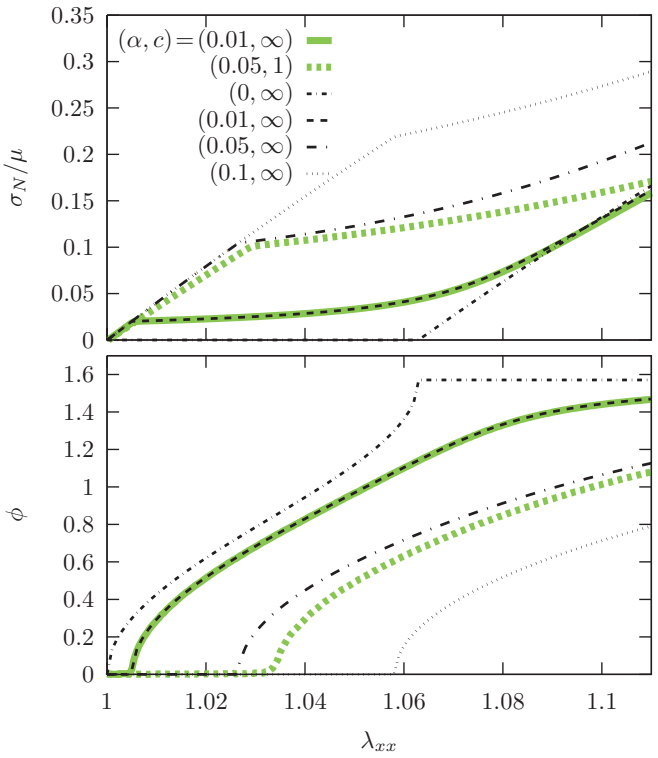

FIG. 7. (Color online) The stress and the angle of rotation of a Sm-C elastomer when stretched perpendicular to both the layer normal and the director. The model parameters are $b = 60$, $r = 2$, $\theta_0 = 0.5$ (radians), and the α and c values shown on the figure. The thick curves (green) are from the more general numerical relaxation, and the black curves are calculated using the decomposition of the deformation matrix explained in the text.

electric dipoles associated with director rotation is spread over a much larger deformation range.

The deformation components when stretching perpendicular to $\mathbf{k}$ are illustrated in Fig. 8. Note that the sympathetic shears that accompany the director rotation are persistent, because the director rotation is never completed if $\alpha > 0$.

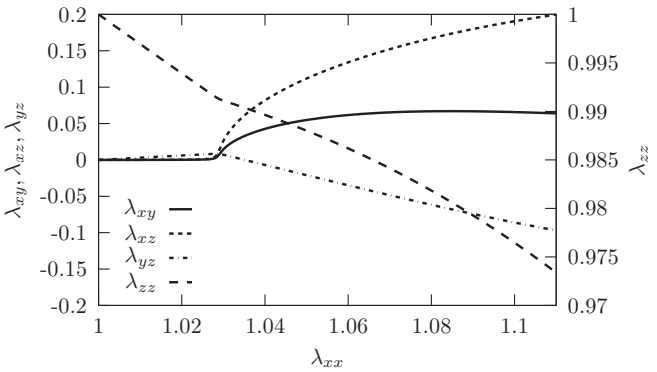

FIG. 8. The components of the deformation tensor for $(\alpha, b, c, \theta_0, r) = (0.05, 60, 1, 0.5, 2)$ when stretching perpendicular to both the director and the layer normal. Note that the sympathetic shears persist, as the director is unable to complete its $\pi/2$ rotation.

Numerically it is clear that with the inclusion of the semisoft term there is a delay in the rotation of the director. Some analytical progress can be made in this geometry by decomposing the deformation into three parts: the initial hard deformation with fixed director and layer spacing denoted $\underline{\underline{\lambda}}_{\text{hard}}$, the soft mode $\underline{\underline{\lambda}}_{\text{soft}}$, and the subsequent shear and elongation after the soft mode $\underline{\underline{\lambda}}'$ [42]

$$\underline{\underline{\lambda}} = \underline{\underline{\lambda}}' \cdot \underline{\underline{\lambda}}_{\text{soft}} \cdot \underline{\underline{\lambda}}_{\text{hard}}, \tag{16}$$

where $\underline{\underline{\lambda}}_{\text{hard}} = \text{diag}(\lambda_1, 1/\lambda_1, 1)$, $\underline{\underline{\lambda}}_{\text{soft}}$ is given in Eq. (5), and

$$\underline{\underline{\lambda}}' = \begin{pmatrix} \zeta & 0 & \eta \\ 0 & 1/\zeta & 0 \\ 0 & 0 & 1 \end{pmatrix}. \tag{17}$$

This deformation matrix can be substituted into the free energy terms of Eqs. (1), (3), and (11) (assuming that $c \to \infty$, so that $\theta = \theta_0$). The problem is then reduced to a minimization over the variables λ_1, ζ, η, and ϕ, with the constraint that the total λ_{xx} is prescribed. The threshold before the onset of director rotation can be calculated by setting $\zeta = 1$ and $\eta = 0$, then performing a series expansion of the free energy in soft mode rotation angle ϕ. The leading term is $O(\phi^2)$, and when this term becomes negative a nonzero value of ϕ will lower the free energy. To leading order in $(\lambda_1 - 1)$, this coefficient becomes negative when λ_1 is approximately

$$\lambda_1 = 1 + 8r^2\alpha/\{1 + 29r - 29r^2 - r^3 + r\alpha + 35r^2\alpha + 4r^2\alpha\cos 2\theta + (r-1)[(r-1)^2 + r\alpha]\cos 4\theta\}. \tag{18}$$

This value is slightly smaller than the corresponding threshold to director rotation in nematic elastomers of $\lambda_1^3 = \frac{r-1}{r-1-\alpha r}$ [1]. Intuitively this is because in the Sm-C phase the deformation is restricted to two dimensions by the layer spacing constraint. Consequently there is a larger contraction in the direction perpendicular to the stretch which causes the elastic free energy to rise faster, and hence the director rotation to start earlier in Sm-C LCEs as compared to the nematic phase.

The minimization of the free energy over λ_1, ζ, η, and ϕ produces results that are in good agreement with the more general numerical method. The results are shown by the black lines in Fig. 7.

B. Elongation parallel to $\mathbf{k}_0$

Elongation parallel to the layer normal is illustrated in Fig. 6(b). The initial layer normal is given by $\mathbf{k}_0 = \mathbf{x}$ and the director $\mathbf{n}_0 = \mathbf{x}\cos\theta_0 + \mathbf{z}\sin\theta_0$. Using the form of deformation matrix described in Eq. (15), the free energy can again be minimized using the numerical technique described in Sec. II C. The results for various values of the semisoft parameter α are illustrated in Fig. 9. For $c \to \infty$ the first part of the stress-strain curve is determined by the smectic layer modulus B. The semisoft term prevents the rotation of the director, and the layer spacing increases. Once the force required to increase the layer spacing is comparable to that required to rotate the director the semisoft mode begins. The stress-strain curve has negative slope once director rotation starts. As explained in Sec. II A there is a negative IPR in this geometry as the director rotates around the layer normal into

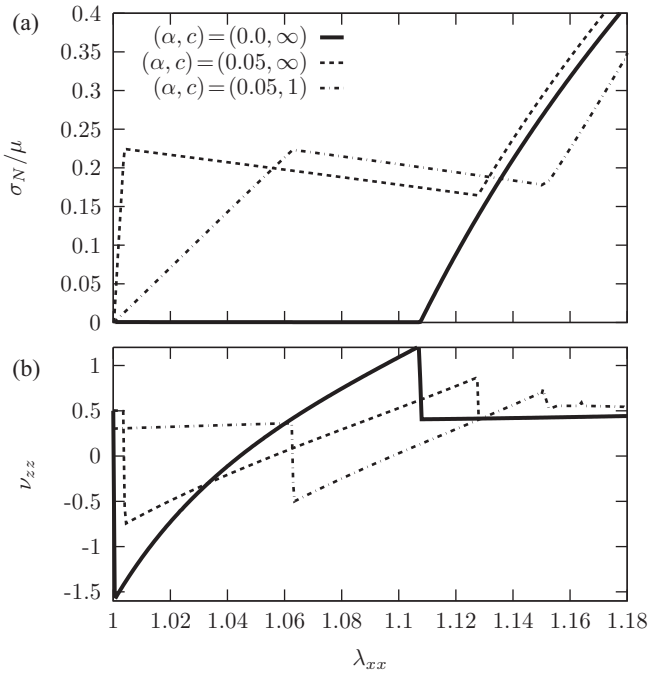

FIG. 9. (a) The stress-strain response for a semisoft Sm-C elastomer stretched parallel to the layer normal. The model parameters are $b = 60$, $r = 2$, and $\theta_0 = 0.5$, and the values of (α, c) shown in the figure. (b) The corresponding IPRs for the stress-strain curves.

the direction perpendicular to the stretch axis [see Fig. 9(b)]. This lateral expansion, combined with the free energy expression for the semisoft elasticity, results in the negative stiffness. For larger values of α the Poisson's ratio becomes less negative.

The rotation of the layer normal and director and the deformation components are illustrated in Fig. 10. The expansion of the sample in the z direction is clearly visible at the onset of rotation, as are the usual shear components that accompany a soft mode. For finite values of c the deformation becomes more complicated; before the threshold the director rotates toward the layer normal and the sample shears, which itself results in movement of the layer normal. There is both an increase in the threshold to the start of rotation and a reduction in the amplitude of the semisoft deformation. This is because the shearing before director rotation results in rotation of the layer normal, and there is a reduction in the tilt angle before the onset of shearing.

1. Scalar model of negative slope region

The unusual response above for the Sm-C soft mode can be illustrated for a much simpler deformation. Consider an elongation with a diagonal deformation matrix of an imposed λ_{xx}, λ_{zz} given by

$$\lambda_{zz} = 1 - A\left(\lambda_{xx} - \frac{3}{2}\right)^2 + \frac{A}{4}, \tag{19}$$

with λ_{yy} determined by volume conservation. The parameter A here controls the initial rate of expansion of the material. Its Poisson's ratios are $-A$ and $1 + A$. This is similar to the

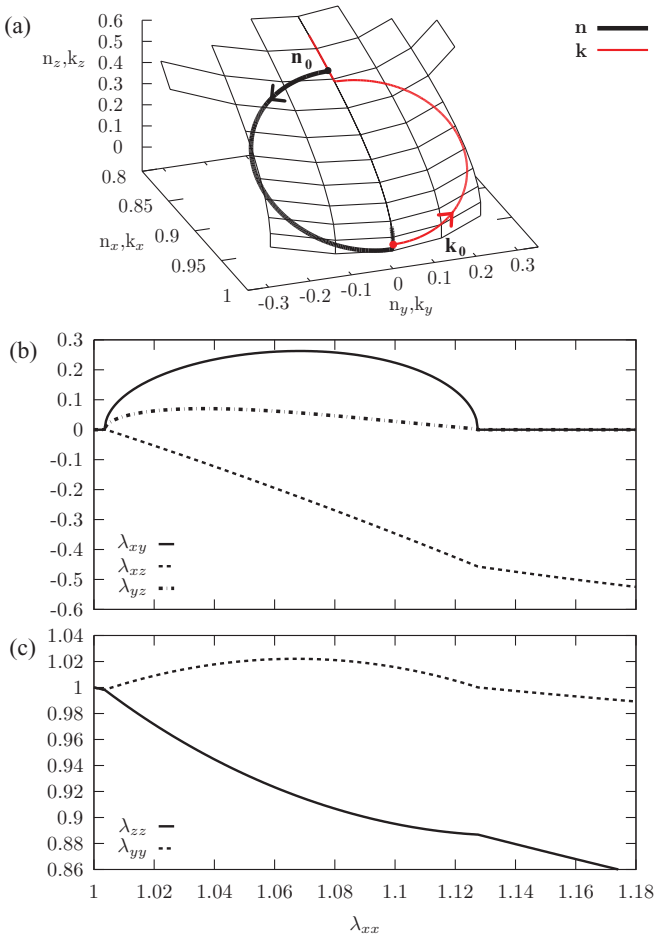

FIG. 10. (Color online) For the parameter values $(\alpha, c) = (0.05, \infty)$ and $b = 60$, $r = 2$, and $\theta_0 = 0.5$ radians for stretching parallel to the layer normal, (a) shows the director (thick black) and layer normal rotation (thin red), (b) the shear components, and (c) the diagonal components of the deformation tensor when stretching parallel to the layer normal.

soft mode in a Sm-C illustrated in Fig. 3. The deformation in Eq. (19) can be substituted into a neo-Hookean model such as Eq. (12), which is broadly similar to the semisoft elastic energy term. The resulting stress-strain curve is shown in Fig. 11. It can be seen from this plot that for sufficiently large values of A the stress-strain curve has a negative slope similar to stretching the Sm-C LCE parallel to the layer normal. For some geometries the Poisson's ratio is sufficiently negative to result in a negative stiffness. The configurational entropy of the perpendicular degrees of freedom decreases as the sample expands resulting in a positive contribution to the stress. Once lateral expansion starts to slow sufficiently there is a weaker contribution to stiffness of the sample from the perpendicular degrees of freedom and the stress starts to drop, which produces a negative slope in the stress-strain response. By tuning the parameter A in the model, the balance between the parallel and perpendicular degrees of freedom can be altered, and the stiffness changed from negative to positive.

This scalar model shows that the negative stiffness is a result of the lateral expansion during the Sm-C soft mode, and not due to the form of the semisoft elastic term.

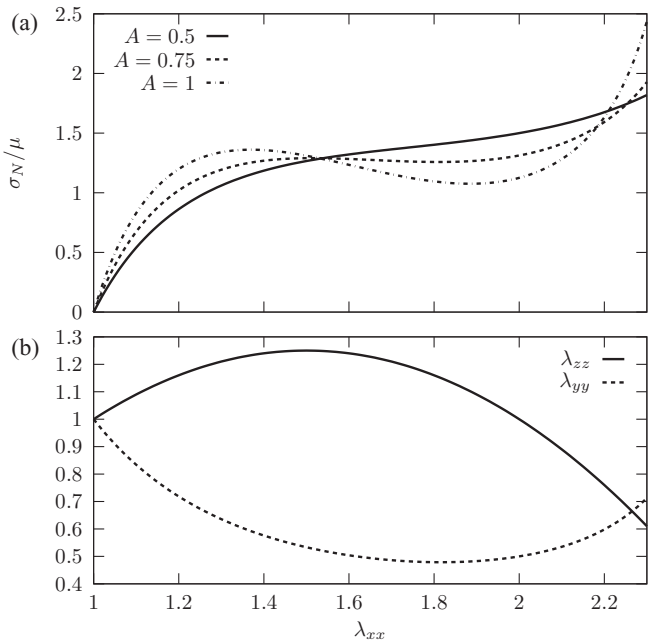

FIG. 11. For the scalar model of the negative stress strain curve described in the text, (a) shows the stress-strain curves for $A = 0.5, 0.75, 1$, and (b) the deformation components for $A = 1$ for the scalar auxetic model.

C. Elongation perpendicular to $\mathbf{n}_0$

Stretching perpendicular to the initial director, $\mathbf{n}_0$ is illustrated in Fig. 6(c). The results for the numerical calculation of the stress-strain curve for this geometry are shown in Fig. 12. This geometry has the remarkable feature that $\nu_{zz} \to -\infty$ when $\alpha \to 0$, as shown in Fig. 12. For larger values of α the Poisson's ratio becomes less negative. The jump in the director also causes a discontinuity in the IPR, and a sudden increase in the width of the sample. Note that in this geometry there is a discontinuity in the stress-strain curve, in addition to the negative stiffness. The discontinuity in the stress-strain curve is accompanied by a jump in the director as shown in Fig. 13. Intuitively the discontinuity arises because when the director jumps the long axis of the polymer shape tensor jumps toward the elongation direction. Consequently the natural length of the rubber in this direction is increased, so there is corresponding drop in the stress.

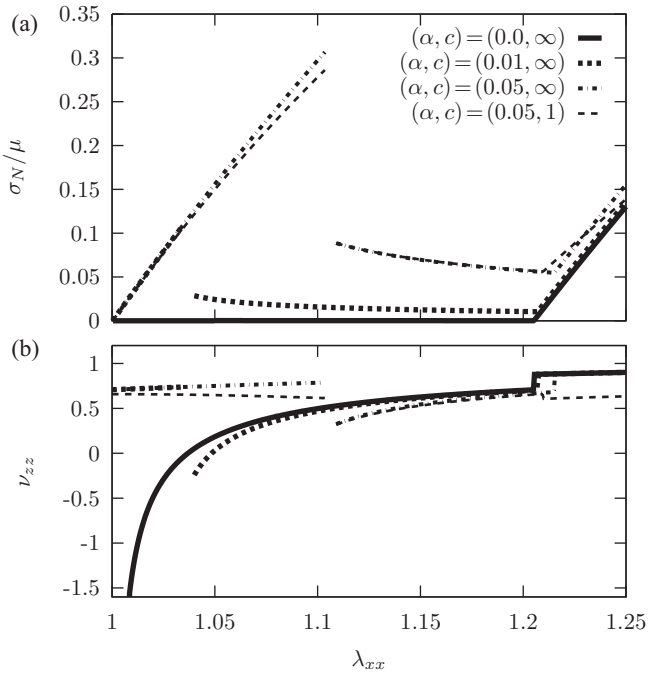

FIG. 12. (a) The stress-strain curves for stretching perpendicular to the layer normal, and (b) the IPR for various parameters $b = 60$, $r = 2$, and $\theta_0 = 0.5$ and values of (α, c) shown in the figure.

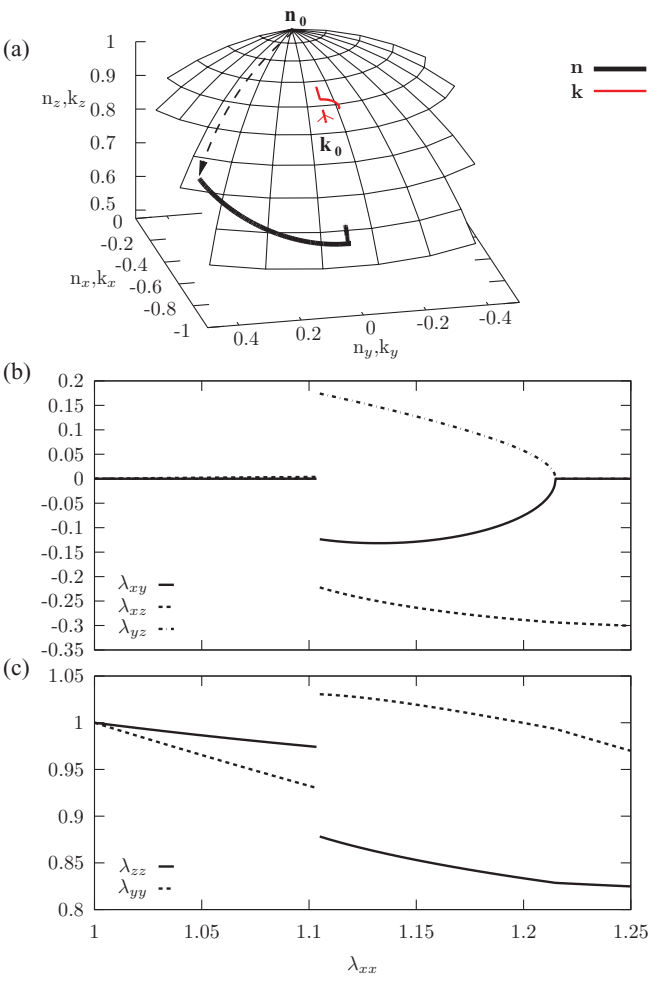

FIG. 13. (Color online) When stretching perpendicular to the director, for the parameter values $(\alpha, c) = (0.05, \infty)$ and $b = 60$, $r = 2$, and $\theta_0 = 0.5$ radians, (a) shows the director (thick black) and layer normal rotation (thin red), (b) the shear components, and (c) the diagonal components of the deformation tensor when stretching perpendicular to $\mathbf{n}_0$.

The jump in the director can be understood from the properties of the soft mode in this geometry. We can approximate the first part of the total deformation (until the end of director rotation) as a hard deformation where there is no director rotation, followed by a soft mode:

$$\underline{\underline{\lambda}} = \underline{\underline{\lambda}}_{\text{soft}} \cdot \underline{\underline{\lambda}}_{\text{hard}}. \tag{20}$$

The soft mode in this geometry can be calculated analytically as explained in Appendix A. While its analytic form is algebraically very long, the amplitude of the soft mode has a much simpler expression, and is given by

$$\lambda_{xx} = \{3 + r(7r - 2) + 4(r^2 - 1)\cos 2\theta_0 + [1 + (2 - 3r)r]\cos 4\theta_0\}^{1/2}/(2\sqrt{2}\rho). \quad (21)$$

The hard part of the deformation has only diagonal elements and an xz shear component:

$$\underline{\underline{\lambda}}_{\text{hard}} = \begin{pmatrix} \lambda_{xx} & 0 & \lambda_{xz} \\ 0 & 1/(\lambda_{xx}\lambda_{zz}) & 0 \\ 0 & 0 & \lambda_{zz} \end{pmatrix}. \quad (22)$$

Substituting this into the full free energy density yields an approximate solution to the minimization problem, where the director rotation is assumed to be continuous. The free energy density in this case is shown in Fig. 14. The analytic solution with continuous director rotation has higher free energy for the first part of the deformation. Hence, the elastomer initially stretches without director rotation. If the director were to start rotating, then the form of the soft mode results in rapid rotation of the director and an infinite slope in the free energy. However, the rate of increase slows, and eventually the state with a rotated director is lower in free energy than that with a fixed director. At this point the director jumps to the new orientation. There is a discontinuity in the slope of the free energy at this point, or equivalently a jump in the stress.

This behavior is not solely a result of the semisoft energy term, but again is a result of the shape of the soft mode, combined with a general semisoft elasticity term. These calculations are based on an equilibrium model of a Sm-C elastomer. A scalar model that displays the same behavior is discussed in Appendix B. In practice kinetic terms, such as viscosity would smooth out the sharp jump demonstrated here.

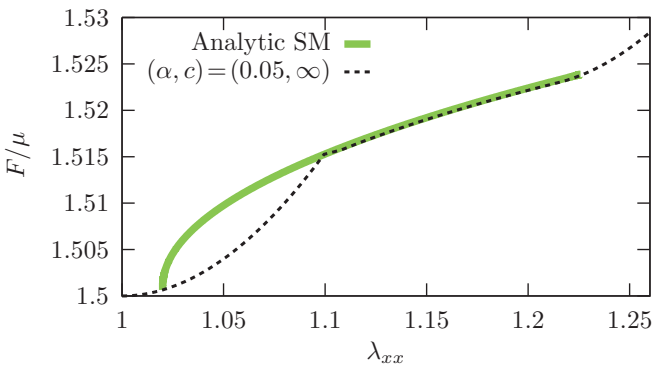

FIG. 14. (Color online) The free energy calculated numerically (dashed black), and the free energy trajectory of the semisoft mode with continuous director rotation (thick green) when stretching perpendicular to the director. Here $b = 60, r = 2, \theta_0 = 0.5$, and (α, c) are shown in the figure.

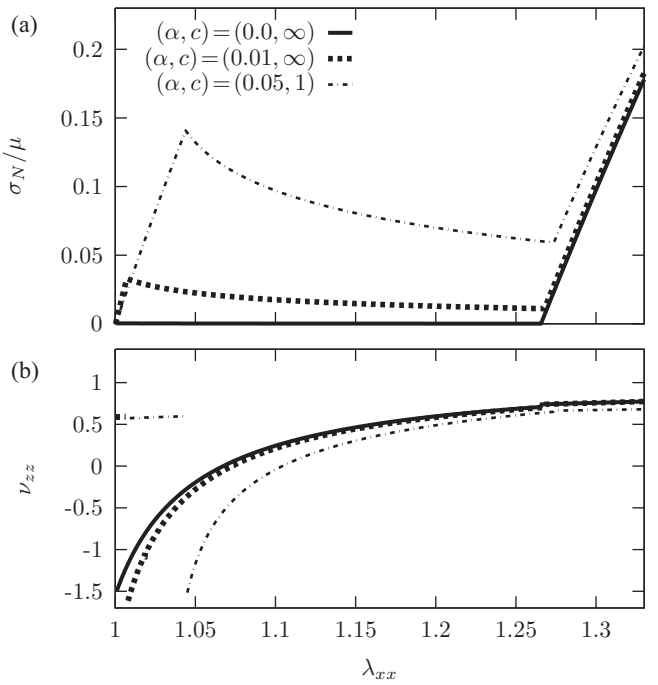

FIG. 15. (a) The stress-strain curves for stretching at an angle of $\psi = 0.65$ radians to the layer normal, for $b = 60, r = 2, \theta_0 = 0.5$ radians, and various parameter values (α, c), and (b) the Poisson's ratio in this geometry.

D. Elongation at an angle ψ to the layer normal

The last deformation we consider is shown in Fig. 6(d). The numerical solution of stress-strain curve associated with this geometry is shown in Fig. 15. The stress-strain curve is continuous in this geometry, but again has a pronounced negative slope. There is a negative IPR of ~ -1.5 that is roughly independent of the semisoft parameter. The expansion of the sample that accompanies the rotation of the director can be seen in Fig. 16.

IV. DISCUSSION

Soft deformations in nematic LCEs are only possible in clamped samples with the formation of microstructure. This has been shown by detailed x-ray experiments [8] and by numerical study [41,43], and is a result of the nonconvex energy of nematic LCEs [44]. The characteristic stress-strain response of Sm-A elastomers [12] also exhibits microstructure if the sample is clamped during stretching [45]. The clamps required in experimental investigation of the Sm-C samples considered here would result in microstructure formation and some changes to the stress-strain response of the material.

The first three deformations considered above in Figs. 6(a)–6(c), when made with clamped boundary conditions, would not be soft even without the semisoft elastic term. This is because no microstructure can be constructed from the soft deformations that is compatible with the boundary conditions, due to the shear components in the Sm-C soft mode [20]. However, the properties of a long sheet of Sm-C LCE may approximate this behavior as the center of the sample could deform without rigid boundary conditions. The

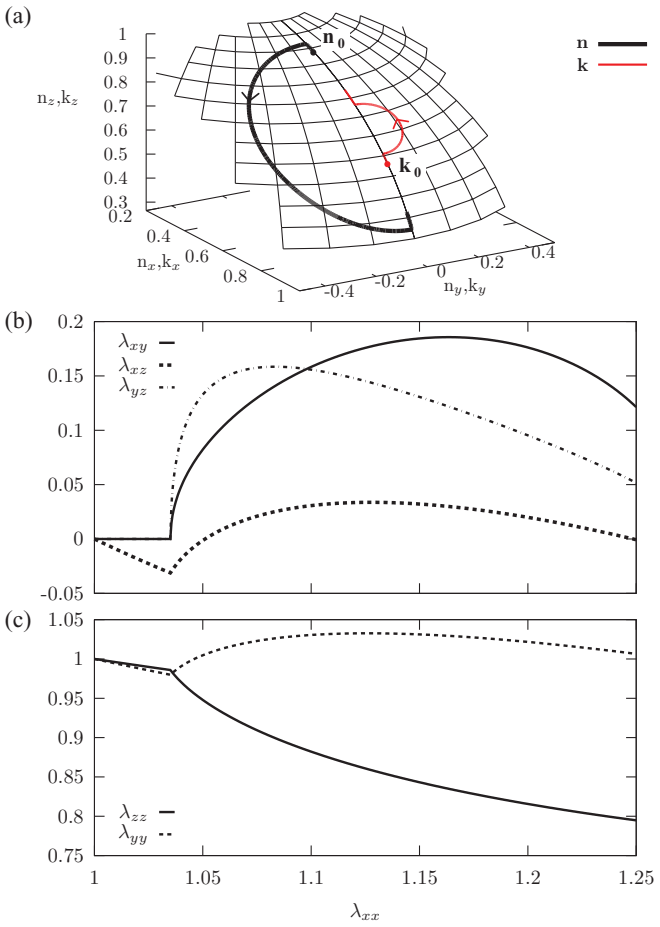

FIG. 16. (Color online) For stretching at an angle of $\psi = 0.65$ radians to the layer normal, (a) shows the director (thick black) and layer normal (thin red), (b) the shear components of the deformation, and (c) the diagonal components of the deformation for stretching at an angle of $\psi = 0.65$ radians to the layer normal, for the case $(\alpha, c) = (0.05, \infty)$ and $b = 60, r = 2, \theta_0 = 0.5$.

final deformation in Fig. 6(d) can be performed with clamped boundary conditions in the soft case. In the semisoft case the sample starts to shear before the onset of rotation, which is not compatible with clamped boundaries, so in experiment it may be even stiffer initially due to this additional constraint on its deformation.

The maximum lateral expansion can be deduced from the soft mode presented in Sec. II A. The shear components are transformed, through a rotation, into an elongation. At $\phi = \pi/2$ the maximum lateral expansion occurs (in the y direction for the example given in the text) and has a value of $\sqrt{r/\rho}$.

The region of negative slope in the constitutive models reported here is typically explained by a Maxwell construction. Similar behavior occurs in the van der Waals gas model which has a region of negative slope in the pressure-volume curve. Here there is a two phase region consisting of a mixture of the liquid and gas phases. In solids the two deformations on either side of the instability must be compatible to form a mixture [46]. The system should then disproportionate, adopting a mixture of the two deformations to achieve the externally imposed strain. The first order type phase transition seen in the example stretching perpendicular to the layer normal can result in hysteretic behavior as the system jumps from one energy well to another. The rate of the deformation in comparison to the sample relaxation times may also result in hysteresis [47].

Experimental work reporting mechanical testing on Sm-C monodomains has not been reported. While it is anticipated that these monodomains should exhibit soft elasticity, the addition of the semisoft elasticity term to the model suggests that these effects may be difficult to observe for large semisoft parameter α. When stretching perpendicular to both the layer normal and the director, the semisoft term may prevent any stress plateau being observed; instead only a shoulder is visible in the stress-strain response.

Although we have only considered the deformations of monodomains here, the results inform model predictions for polydomains. Polydomains are difficult to model because of the requirement of ensuring that adjacent domains deform in a compatible way. A simplifying approximation used to model a polydomain is to assume that it consists of an array of monodomains that deform at the imposed external strain, but are independent from each other. If we deform the pseudo-monodomain shown in Fig. 1 by stretching in the **x** direction, then deformation component λ_{yy} averaged over all the domains is illustrated in Fig. 17 for 50 domains. This figure shows that there is a negative IPR as the director in each of the domains jumps causing them to expand. The curve illustrated here is jagged because the alignment of each domain jumps at a slightly different threshold. The expansion of the film thickness and the energy loss as a result of the jump in the director orientation in this geometry may be observable in experiments on pseudo-monodomains [11,48]. The larger values of deformation reported in experiment before the knee in the stress-strain curve point to a much larger value of α than in the illustrative plot in Fig. 17.

The features of the Sm-C model described here would be present in a wide range of models that have soft modes of nematic elastomers but incorporate the constraint on the director to remain at a fixed angle to the layer normal. However, validation of these models awaits either experimental work on mechanical testing of Sm-C monodomains or theoretical work

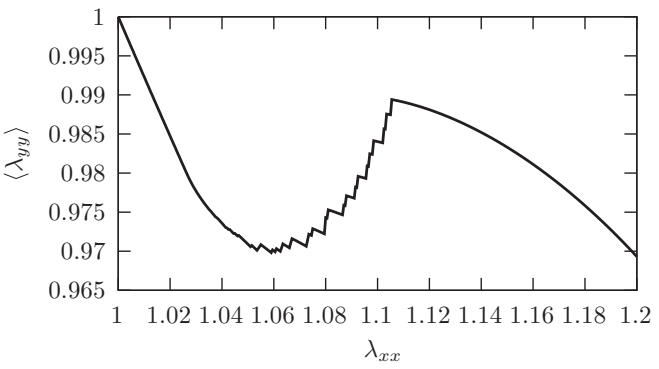

FIG. 17. The average value of λ_{yy} for 50 domains in a pseudo-monodomain illustrated in Fig. 1 as a function of λ_{xx} assuming they all experience the same strain and deform independently. Model parameters are $b = 60, r = 2, \theta_0 = 0.5, c = \infty, \alpha = 0.05$.

on pseudo-monodomains to link up with existing mechanical experiments on pseudo-monodomains.

V. CONCLUSION

We have studied a model of monodomain Sm-*C* LCEs with the inclusion of a semisoft elastic term to describe imperfections in the elastomer. As result of the negative incremental Poisson's ratio inherent in the soft modes of a Sm-*C* monodomain, the mechanical properties of a semisoft monodomain are unusual. When stretching perpendicular to the layer normal and the director, the response is reminiscent of a nematic elastomer. A finite force is required to deform the LCE and initiate the rotation of the director. However, the stress plateau is less well defined for larger values of semisoft parameter α; it is reduced to a shoulder in the stress-strain response. This is at variance to the nematic case where the plateau in the stress-strain response remains, even in the limit of large α. When stretching parallel to the layer normal the elastomer again exhibits a threshold to director rotation. Once director rotation has started the elastomer has a negative incremental Poisson's ratio and a negative stiffness. A negative incremental Poisson's ratio of up to $\nu \sim -1.5$ has been found for typical model parameters. This arises because the director rotates in a direction perpendicular to the stretch axis due to the constraint of the layer normal. This more detailed understanding of monodomain deformations of Sm-*C* elastomers might prove useful in understanding recent mechanical and piezoelectric experiments on polydomain Sm-*C* elastomers.

ACKNOWLEDGMENTS

We would like to thank SEPnet for supporting this project, and Dr. Daniel Corbett and Dr. James Busfield for helpful discussions.

APPENDIX A: TRANSFORMING THE SOFT MODE FOR DIFFERENT STARTING CONFIGURATIONS

The soft mode given by Eq. (5) can be transformed to other geometries by a pair of rotation matrices. For example, consider the case of a Sm-*C* elastomer stretched parallel to the layer normal. Let us assume that starting layer normal is $\mathbf{k}_0 = \mathbf{x}$ and the starting director is $\mathbf{n}_0 = \cos\theta_0\mathbf{x} + \sin\theta_0\mathbf{y}$. The soft mode for this configuration that is an upper triangular matrix, as described in Eq. (15), can be found as follows. From the reference configuration a body rotation is performed such that the layer normal $\mathbf{k}_0$ is parallel to the $\mathbf{z}$ axis. In this case, a 90° rotation about the $\mathbf{y}$ axis

$$\underline{\underline{Q}} = \begin{pmatrix} 0 & 0 & -1 \\ 0 & 1 & 0 \\ 1 & 0 & 0 \end{pmatrix}. \tag{A1}$$

After this rotation the director is given by $\mathbf{n} = \mathbf{z}\cos\theta_0 + \mathbf{y}\sin\theta_0$. Note that in general an additional rotation around the $\mathbf{z}$ axis may be required to ensure the director is in this orientation. This is the initial configuration for the soft mode given in Eq. (5). The director now rotates by an angle ϕ around the new layer normal, and the sample executes the soft mode. Finally a rotation of the target state is performed such that the deformation matrix has the form described in Eq. (15). This rotation matrix is in general simpler if we first undo the rotation $\underline{\underline{Q}}$. The rotation matrix $\underline{\underline{P}}$ is described by three angles:

$$\underline{\underline{P}} = \begin{pmatrix} \cos\psi_z & \sin\psi_z & 0 \\ -\sin\psi_z & \cos\psi_z & 0 \\ 0 & 0 & 1 \end{pmatrix} \cdot \begin{pmatrix} 1 & 0 & 0 \\ 0 & \cos\psi_x & \sin\psi_x \\ 0 & -\sin\psi_x & \cos\psi_x \end{pmatrix} \cdot \begin{pmatrix} \cos\psi_y & 0 & \sin\psi_y \\ 0 & 1 & 0 \\ -\sin\psi_y & 0 & \cos\psi_y \end{pmatrix}. \tag{A2}$$

The three angles ψ_x, ψ_y, and ψ_z can be calculated by substituting into the equation

$$\underline{\underline{\lambda}} = \underline{\underline{P}} \cdot \underline{\underline{Q}}^T \cdot \underline{\underline{\lambda}}_{\text{soft}} \cdot \underline{\underline{Q}} \tag{A3}$$

and ensuring that the three lower triangular elements of $\underline{\underline{\lambda}}$ are zero. In the case of stretching parallel to $\mathbf{k}_0$ and perpendicular to $\mathbf{n}_0$ the soft mode can be calculated analytically. The algebraic expression for these soft modes is long and unedifying so will not be presented here.

APPENDIX B: SCALAR MODEL DESCRIBING STRESS DISCONTINUITY

The semisoft behavior of Sm-*C* elastomers is characterized by two deformation modes: before the onset of director rotation and afterward. A scalar model that exhibits the same behavior when stretching perpendicular to the director can be developed based on representing each of these deformation modes as a spring, and deforming the two springs in series. The total strain is the sum of two deformation modes corresponding to keeping a fixed director ϵ_{U} and rotating the director ϵ_{SM}:

$$\epsilon_{\text{T}} = \epsilon_{\text{U}} + \epsilon_{\text{SM}}. \tag{B1}$$

The two modes of deformation have different energy penalties. The first arises from a simple uniaxial deformation, so in a neo-Hookean energy model will result in a free energy term of the form

$$F_{\text{U}} = \tfrac{1}{2}K_1\epsilon_{\text{U}}^2, \tag{B2}$$

where K_1 corresponds to the shear modulus of the rubber. The second arises from the soft mode, which has a singular edge in the contraction of the rubber as it is stretched. The zz component in the soft mode is initially of the form $\lambda_{zz} = 1/[1 + (\lambda_{xx} - 1)^{\beta}]$ (where here $\lambda_{xx} - 1 = \epsilon_{\text{SM}}$). When this is put into the neo-Hookean free energy, it results in free energy terms to leading order in ϵ_{SM} of the form

$$F_{\text{SM}} = \tfrac{1}{2}K_2\epsilon_{\text{SM}}^{\beta}, \tag{B3}$$

where K_2 is the corresponding shear modulus for this mode. In the case of the semisoft Sm-*C* elastomer, this term arises because of the rapid rotation of the director during the start of the soft mode.

The total free energy is then

$$F_{\text{T}} = \tfrac{1}{2}K(\epsilon_{\text{T}} - \epsilon_{\text{SM}})^2 + \tfrac{1}{2}K_2\epsilon_{\text{SM}}^{\beta}, \tag{B4}$$

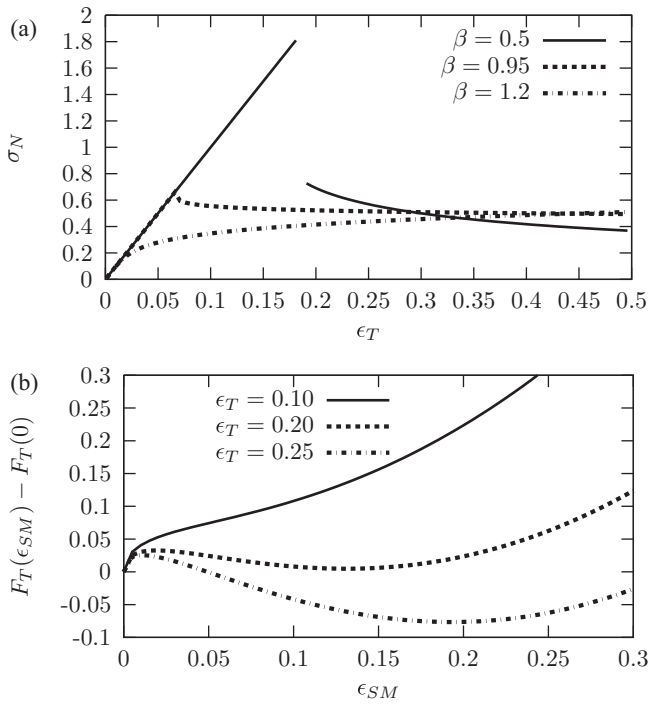

FIG. 18. (a) An illustration of a discontinuous stress-strain curve for the scalar model described in the text. (b) The free energy as a function of the variable ϵ_{SM} for fixed total strain values. Here $K_1 = 10$ and $K_2 = 1$.

where the first spring in this system is Hookean and the second is nonlinear, being infinitely stiff at zero strain for $0 < \beta < 1$, but softening rapidly as strain increases. This should be minimized over ϵ_{SM} to determine the distribution of strain between the two springs. It can be solved analytically for $\beta = 0.5$. The behavior of this model is illustrated in Fig. 18. For small β this system has a discontinuity in the stress-strain curve, but as β is increased the stress-strain response becomes continuous. The free energy as a function of ϵ_{SM} is also illustrated in Fig. 18. For small values of ϵ_T there is only one minimum at $\epsilon_{SM} = 0$, corresponding to no strain of the second spring. However, as the total strain increases, the second mode of deformation becomes activated and there is a minimum for larger values of ϵ_{SM}. Since there is a barrier between the two minima, the transition is first order, so there is a jump in the equilibrium value of ϵ_{SM}. For larger values of β the phase transition becomes continuous, and the stress-strain curve no longer exhibits a jump.

This behavior is analogous to that of the semisoft Sm-*C* elastomer as the free energy exhibits a discontinuity when stretched perpendicular to the director (where the soft mode has a singular edge). Larger values of β correspond to stretching at a larger angle to the director, where the soft mode does not have such a rapid rotation of the director, and a corresponding sharp drop in the lateral dimension. If the angle between the director and the elongation direction is small enough, then the stress-strain response becomes continuous as in Sec. III D.

[1] M. Warner and E. M. Terentjev, *Liquid Crystal Elastomers* (Oxford University Press, Oxford, 2007).
[2] M. Warner, P. Bladon, and E. M. Terentjetv, J. Phys. (Paris) II **4**, 93 (1994).
[3] I. Kundler and H. Finkelmann, Macromol. Rapid Commun. **16**, 679 (1995).
[4] S. M. Clarke, E. M. Terentjev, I. Kundler, and H. Finkelmann, Macromolecules **31**, 4862 (1998).
[5] J. S. Biggins, M. Warner, and K. Bhattacharya, Phys. Rev. Lett. **103**, 037802 (2009).
[6] K. Urayama, Macromolecules **40**, 2277 (2007).
[7] H. Finkelmann, I. Kundler, E. M. Terentjev, and M. Warner, J. Phys. (Paris) II **7**, 1059 (1997).
[8] E. R. Zubarev, S. A. Kuptsov, T. I. Yuranova, R. V. Talroze, and H. Finkelmann, Liq. Cryst. **26**, 1531 (1999).
[9] A. DeSimone and G. Dolzmann, Arch. Ration. Mech. Anal. **161**, 181 (2002).
[10] J. S. Biggins, E. M. Terentjev, and M. Warner, Phys. Rev. E **78**, 041704 (2008).
[11] A. Sánchez-Ferrer and H. Finkelmann, Macromolecules **41**, 970 (2008).
[12] E. Nishikawa and H. Finkelmann, Macromol. Chem. Phys. **200**, 312 (1999).
[13] J. M. Adams and M. Warner, Phys. Rev. E **71**, 021708 (2005).
[14] O. Stenull and T. C. Lubensky, Phys. Rev. E **76**, 011706 (2007).
[15] E. Nishikawa and H. Finkelmann, Macromol. Rapid Commun. **18**, 65 (1997).
[16] C. M. Spillmann, J. H. Konnert, J. M. Adams, J. R. Deschamps, J. Naciri, and B. R. Ratna, Phys. Rev. E **82**, 031705 (2010).
[17] E. P. Obraztsov, A. S. Muresan, B. I. Ostrovskii, and W. H. de Jeu, Phys. Rev. E **77**, 021706 (2008).
[18] J. M. Adams and M. Warner, Phys. Rev. E **72**, 011703 (2005).
[19] O. Stenull and T. C. Lubensky, Phys. Rev. E **74**, 051709 (2006).
[20] J. Adams, S. Conti, and A. DeSimone, Continuum Mech. Thermodyn. **18**, 319 (2007).
[21] J. Küpfer and H. Finkelmann, Makromolekulare Chemie, Rapid Commun. **12**, 717 (1991).
[22] P. Heinze and H. Finkelmann, Macromolecules **43**, 6655 (2010).
[23] K. Semmler and H. Finkelmann, Macromol. Chem. Phys. **196**, 3197 (1995).
[24] K. Hiraoka and H. Finkelmann, Macromol. Rapid Commun. **22**, 456 (2001).
[25] K. Hiraoka, W. Sagano, T. Nose, and H. Finkelmann, Macromolecules **34**, 7352 (2005).
[26] A. Sánchez-Ferrer and H. Finkelmann, Macromol. Rapid Commun. **32**, 309 (2011).
[27] R. Ishige, K. Osada, H. Tagawa, H. Hiwano, M. Tokita, and J. Wantanabe, Macromolecules **41**, 7566 (2008).
[28] J. M. Adams and M. Warner, Phys. Rev. E **79**, 061704 (2009).
[29] P. Papadopoulos, P. Heinze, H. Finkelmann, and F. Kremer, Macromolecules **43**, 6666 (2010).
[30] Y. H. Na, Y. Aburaya, H. Orihara, and K. Hiraoka, Phys. Rev. E **83**, 061709 (2011).

[31] R. Lakes, Science **235**, 1039 (1987).
[32] R. S. Lakes, T. Lee, A. Bersie, and Y. C. Wang, Nature (London) **410**, 565 (2001).
[33] N. Fang, D. J. Xi, J. Y. Xu, M. Ambati, W. Srituravanich, C. Sun, and X. Zhang, Nature Mater. **5**, 452 (2006).
[34] J. M. Adams and M. Warner, Phys. Rev. E **73**, 031706 (2006).
[35] O. Stenull, T. C. Lubensky, J. M. Adams, and M. Warner, Phys. Rev. E **78**, 021705 (2008).
[36] D. Kramer and H. Finkelmann, Phys. Rev. E **78**, 021704 (2008).
[37] A. DeSimone, Ferroelectrics **222**, 275 (1999).
[38] W. T. Ren, Ph.D. thesis, Georgia Institute of Technology, 2007.
[39] W. Ren, P. J. McMullan, and A. C. Griffin, Phys. Status Solidi B **9**, 2124 (2009).
[40] A. DeSimone and L. Teresi, Eur. Phys. J. E **29**, 191 (2009).
[41] S. Conti, A. DeSimone, and G. Dolzmann, J. Mech. Phys. Solids **50**, 1431 (2002).
[42] J. M. Adams and M. Warner, Phys. Rev. E **77**, 021702 (2008).
[43] S. Conti, A. DeSimone, and G. Dolzmann, Phys. Rev. E **66**, 061710 (2002).
[44] P. Cesana and A. DeSimone, J. Mech. Phys. Solids **59**, 787 (2011).
[45] J. Adams, S. Conti, and A. DeSimone, Math. Models Methods Appl. Sci. **18**, 1 (2008).
[46] J. M. Adams, M. Warner, O. Stenull, and T. C. Lubensky, Phys. Rev. E **78**, 011703 (2008).
[47] G. S. Agarwal and S. R. Shenoy, Phys. Rev. A **23**, 2719 (1981).
[48] W. Ren, P. J. McMullan, and A. C. Griffin, Macromol. Chem. Phys. **209**, 1896 (2008).